FULL PAPER

Synthesis of ZIF-93/11 Hybrid Nanoparticles *via* Post-synthetic modification of ZIF-93 and their Use for H_2/CO_2 Separation

Javier Sánchez-Laínez,[a] Beatriz Zornoza,[a] Angelica F. Orsi,[b] Magdalena M. Łozińska,[b] Daniel M. Dawson,[b] Sharon E. Ashbrook,[b] Sthephen M. Francis,[b] Paul A. Wright,[b] Virginie Benoit,[c] Philip L. Llewellyn,[c] Carlos Téllez[a] and Joaquín Coronas[a*]

Abstract: The present work shows the synthesis of nano-sized hybrid zeolitic imidazolate frameworks (ZIFs) with the **rho** topology based on a mixture of the linkers benzimidazole (bIm) and 4-methyl-5-imidazolecarboxaldehyde (4-m-5-ica). The hybrid ZIF was obtained *via* post-synthetic modification of ZIF-93 in a bIm solution. The use of different solvents, MeOH and DMAc, and reaction times led to differences in the quantity of bIm incorporated to the framework, from 7.4 to 23% according to solution-state NMR spectroscopy. XPS analysis showed that the mixture of linkers was also present at the surface of the particles. The inclusion of bIm to the ZIF-93 nanoparticles improved the thermal stability of the framework and also increased the hydrophobicity according to water adsorption results. N_2 and CO_2 adsorption experiments revealed that the hybrid material has an intermediate adsorption capacity, between those of ZIF-93 and ZIF-11. Finally, ZIF-93/11 hybrid materials were applied as fillers in polybenzimidazole (PBI) mixed matrix membranes (MMMs). These MMMs were used for H_2/CO_2 separation (at 180 ^{0}C) reaching values of 207 Barrer of H_2 and a H_2/CO_2 selectivity of 7.7 that clearly surpassed the Robeson upper bound (corrected for this temperature).

Introduction

Zeolitic imidazolate frameworks (ZIFs) are crystalline structures where imidazolate linkers join tetrahedral Zn (II) or Co (II) centres, building metal–imidazole–metal angles close to 145°, similar to the Si–O–Si angles typically found in zeolites. They are a class of metal-organic frameworks (MOFs) with high porosity and good thermal and chemical stability. A large number of potential applications have been developed with them, such as gas sorption,[1] gas separation,[2] drug delivery[3] and catalysis.[4]

A significant number of ZIFs have been reported since the first frameworks were discovered by Yaghi's group in 2006.[5] Among them, new hybrid structures with a combination of different linkers in the same framework have been deduced. Preparation of these mixed linker, hybrid structures of ZIFs by solvothermal synthesis can be found in the literature. Thompson *et al.* [6] reported the synthesis for the ZIF-7/90 and ZIF-7/8 hybrids. In their work, the combined frameworks were obtained by reactions in DMF/MeOH mixtures with fixed amounts of the metal source and both linkers (benzimidazole (bIm) and carboxaldehyde-2-imidazole for ZIF-7/90, and bIm and 2-methylimidazole for ZIF-7/8). The ZIF-7/8 hybrid has also been synthesised using Co(II) as the metal source (ZIF-9/67).[7] The resulting hybrid ZIFs contained a combination of the different linkers in different proportions. Furthermore, the series ZIF-68 to ZIF-70,[8] ZIF-78 to ZIF-82[9] and ZIF-300 to ZIF-302[10] comprise hybrid ZIFs with mixtures of linkers in their structure (2-methylimidazole or 2-nitroimidazole with benzimidazole derivatives). The latter series has the **cha** topology and the other two sets have the **gme** topology.

The direct synthesis of hybrid frameworks may not be always possible. Problems arising from limited linker solubility, chemical and thermal stability, or functional group compatibility can make the direct synthesis of hybrid ZIFs difficult. Post-synthetic modification routes are, therefore, a useful alternative approach. Through this technique, materials of high complexity and functionality can be obtained providing the MOF is not destroyed during the chemical reaction. Post-synthetic modification of MOFs can be classified into three types: covalent, dative and post-synthetic deprotection.[11] Covalent post-synthetic modification involves the use of a reagent to modify a component of the original MOF (generally the organic linker) to form a new covalent bond. In dative post-synthetic modification, the reagent modifies the MOF forming a dative bond instead and usually a new linker or a metal source is incorporated to the framework in this manner. Finally, in post-synthetic deprotection the destruction of a target

[a] J. Sánchez-Laínez, Dr. B. Zornoza, Prof. Dr. C. Téllez, Prof. Dr. J. Coronas.
Chemical and Environmental Engineering Department, Instituto de Nanociencia de Aragón(INA), Universidad de Zaragoza, 50018 Zaragoza, Spain. Email: coronas@unizar.es

[b] Dr. A. F. Orsi, M. M. Łozińska, D. M. Dawson, Prof. S. E. Ashbrook, S. M. Francis, Prof. Dr. P. A. Wright.
Eastchem School of Chemistry, University of St. Andrews, St. Andrews, Fife KY16 9ST, United Kingdom

[c] Dr. V. Benoit, Dr. P. L. Llewellyn
Aix Marseille University, CNRS, MADIREL, UMR 7246, 13397 Marseille, France

Supporting information for this article is given via a link at the end of the document

chemical bond inside an intact MOF results in the *in-situ* formation of a linker with new chemical functionality.

Post-synthetic modification has been successfully applied for many MOFs, including: IRMOF-3[12], MIL-53(Al),[13] MIL-53(Al)-NH_2,[14] MIL-101(Fe)-NH_2,[15] MIL-101(Cr),[16] UiO-66-NH_2,[17] UiO-66-Br[18] and HKUST-1.[19] Post-synthetic modification of ZIFs have also been demonstrated. Examples include the conversion of SIM-1 (also known as ZIF-94) to ZIF-91 and ZIF-92 (using $NaBH_4$ and ethanolamine, respectively),[20] the conversion of SIM-1 to SIM-2(C_{12}) using dodecylamine,[21] and the transformation of SIM-1 to ZIF-93 upon post-synthetic functionalization with amines.[22] Furthermore, Liu *et al.*[23] modified ZIF-8 *via* a shell-linker-exchange reaction in MeOH with different imidazole-like linkers, obtaining a core-shell structure with improved hydrothermal stability relative to the parent material. Very recently our group also developed the synthesis of ZIF-7/8 core-shell materials by post-synthetic modification.[24] These modification results of ZIFs represent an interesting way of controlling the particle size, chemical function, adsorption property and pore size.

In the context of gas separation, it is of great importance that the framework has narrow porosity, especially when operating at high temperature, at which adsorption capacities are almost negligible, and the sieving process gains importance. This is the case for H_2/CO_2 mixtures typically obtained at high pressure and temperature during hydrogen production *via* steam reforming of methane. One of the most interesting ZIFs for this gas separation is ZIF-11 (**rho** framework of Zn(II) centres connected by bIm units), which has small pore windows of 0.30 nm diameter that are intermediate between the kinetic diameters of H_2 and CO_2 (0.29 and 0.33 nm, respectively). Simulation results have shown that this ZIF can achieve a H_2/CO_2 selectivity of 262.[25] ZIF-93 is another Zn(II)-based **rho-**type framework composed of 4-m-5-ica organic linker with pore size 0.36 nm[26] and a high CO_2 uptake.[27]

The removal of CO_2 from H_2 is a critical requirement for hydrogen to be a sustainable energy system as well as for the minimisation of environmental impact, since it is a well-known pollutant. Among the different technologies for H_2/CO_2 separation, membrane technology is an alternative to other established methods such as amine-based absorption, pressure-swing adsorption or cryogenic distillation.[28] However this approach faces the challenge that both molecules have a similar kinetic diameter. The use of mixed matrix membranes (MMMs) is a widespread approach to enhance the H_2 selectivity of polymeric membranes.[29] MMMs comprise the dispersion of generally porous fillers into a polymeric phase. The resulting membrane combines the advantageous properties of both phases: the good processability of polymers and the highest gas separation capacity of the filler. MOFs are particularly suitable as fillers as, owing to their partial organic nature, they show a better affinity for the polymeric chains than wholly inorganic fillers. In addition, the MOF-polymer interface interactions are easier to control in order to avoid non-selective voids between the phases. Thus, MOFs have often been used in MMMs over the last few years.[2a]

The use of polybenzimidazole (PBI) membranes for the separation of H_2/CO_2 mixtures has been widely reported.[30] PBI is a polymer with high thermal stability, good chemical resistance, impressive compression strength and high intrinsic H_2/CO_2 selectivity. However, its major drawbacks are low permeability and brittleness.[31] Several types of ZIFs, such as ZIF-7,[30b] ZIF-8,[32] ZIF-11,[30c, 33] and ZIF-90[34] have been embedded in the PBI continuous phase. However, to date there have been no reports of the use of ZIF-93 for this purpose.

In the present work we show the synthesis of a ZIF-93/11 hybrid material prepared from ZIF-93 nanoparticles following a post-synthetic modification route in different solvents. The post-synthetic method allowed a better control of the particle size and relative proportions of bIm and 4-m-5-ica (bIm/4-m-5-ica) than a direct synthesis. The nanoparticles were characterized by several techniques to study their physical and chemical properties. Finally, two types of hybrids were embedded in a commercial PBI continuous phase in the form of MMMs that were tested at high temperature (180 ^{0}C) to evaluate their performance in the separation of the H_2/CO_2 mixture.

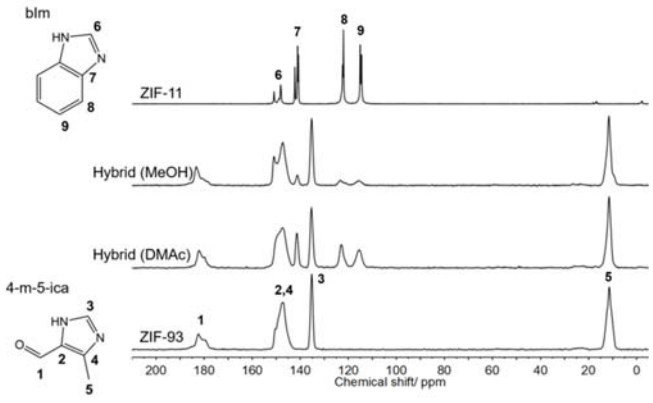

Figure 1. Solid-state ^{13}C CP MAS NMR spectra of ZIF-93 (bottom), hybrid materials synthesised in DMAc and MeOH (middle) and ZIF-11 (top). ZIF-93, ZIF-11 and hybrid synthesised in DMAc were washed in MeOH and dried prior to analysis.

Results and Discussion

ZIF characterisation

The presence of both 4-methyl-5-imidazolecarboxaldehyde (4-m-5-ica) and benzimidazole (bIm) linkers inside the ZIF-93/11 framework structure, as well as their proportion, was determined by solution-state NMR analysis. Solution-state ^{1}H-NMR spectra (Figures S1 and S2) of the digested ZIF-93/-11 hybrid materials confirmed that both linkers were present. Integration of signals of the aldehyde proton (H-1) of 4-m-5-ica and the imidazole ring proton (H-4) of bIm resulted in linker ratios of 3.3:1 and 12.5:1 for the hybrid materials synthesised in DMAc and MeOH, respectively (Table S1). The hybrid material synthesised in DMAc has more bIm linker present (23%) compared to the sample synthesised in MeOH (7.4%). This agrees with a higher solubility of the outgoing ligand (4-m-5-ica) in DMAc than in MeOH. To prove this, the calculated value of the solubility parameter Ra of 4-m-5-ica in DMAc is 6.6, while it is of 14.9 in MeOH (both calculated with the Equation S1 using the Hansen Solubility Parameters (HSP) of Table S2).[35]

Solid-state ^{13}C CP MAS NMR spectra (Figure 1) were acquired for ZIF-93, ZIF-11 and the two hybrid materials synthesised in DMAc and MeOH solvents. Prior to analysis ZIF-93, ZIF-11 and the hybrid material synthesised in DMAc were washed in MeOH

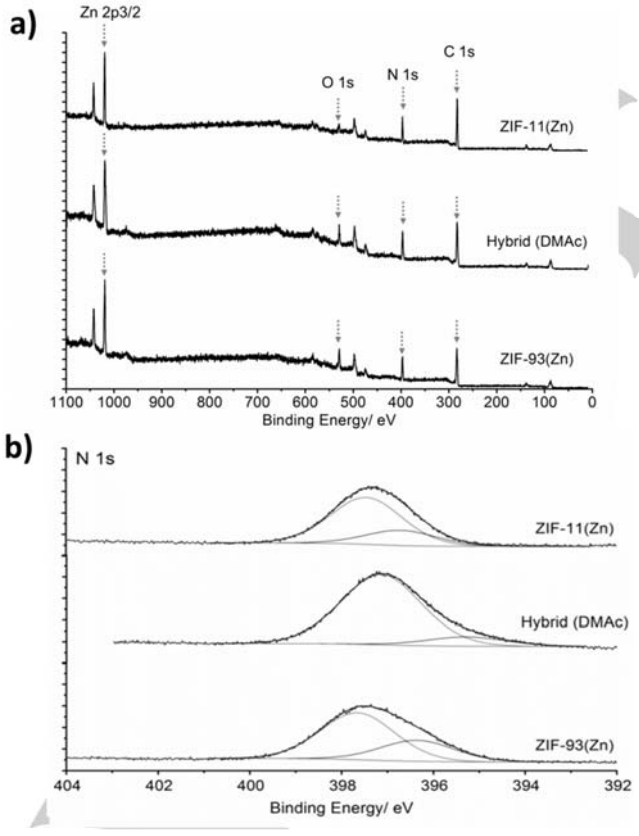

Figure 2. XPS survey scans (a) of ZIF-93, the hybrid material synthesised in DMAc and ZIF-11. The N 1s component region of the XPS spectra (b) of ZIF-93, the hybrid material synthesised in DMAc and ZIF-11.)

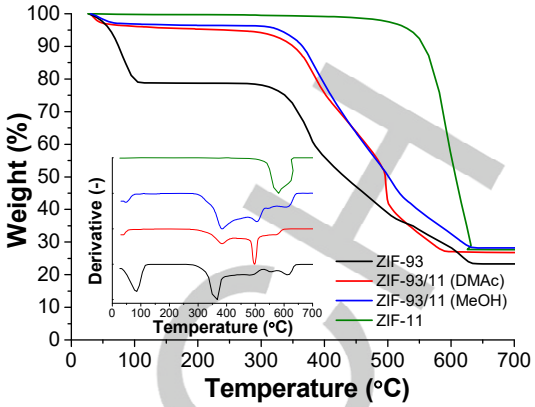

Figure 3. TGA curves and derivatives (inset) in flowing air. From bottom to top: ZIF-93 (black), ZIF-93/11 hybrid (DMAc) (red), ZIF-93/11 hybrid (MeOH) (blue) and ZIF-11 (green).

(1 day) to remove residual solvents. The carbons of the 4-m-5-ica linker of ZIF-93 and the bIm linker of ZIF-11 are present in the spectra of the hybrid materials. The intensity of the bIm carbon signals in the hybrid material synthesised in MeOH are lower than those in the material synthesised in DMAc, which agrees well with the results from solution-state ^{1}H-NMR. The linewidths for the ^{13}C signals in ZIF-11 have high resolution, indicating ordered linkers in the framework. ZIF-93 has much broader ^{13}C signals suggesting orientational disorder of the linkers in the framework. The bIm signals in the hybrid materials are broadened compared to those in ZIF-11, suggesting that disorder of the 4-m-5-ica linkers also affects the ZIF-11 areas of the hybrid materials. This confirms that the two linkers are within the same particles and that there is not a sharp border separating both ZIF structures.

XPS analysis was performed to study the external surface of ZIF-93, ZIF-11 and the hybrid materials synthesised in DMAc (that with the highest concentration of bIm according to the NMR spectra). XPS is a surface sensitive technique, probing 1-12 nm thickness. The XPS survey scans as well as the N 1s component region of the XPS spectra in Figure 2 showed little difference between the surfaces of ZIF-93, ZIF-11 and the hybrid material. This agrees with the chemical similarity of both imidazolate ligands and with the bIm minority presence in both MeOH and DMAc hybrids (7.4-23%, as seen above).

Thermogravimetric analyses (TGA) in flowing air were used to elucidate the thermal stability of the different materials prepared in this work: ZIF-93, ZIF-11 and both hybrid materials. The results can be seen in Figure 3. ZIF-93 shows four clear decomposition steps at 366, 484, 554 and 612 ^{0}C corresponding to the progressive degradation of its 4-m-5-ica linker (ZIF-93 is highly hygroscopic and the mass loss below 200 ^{0}C corresponds to the loss of the ~20 wt% adsorbed water). ZIF-11 shows a higher onset temperature (576 ^{0}C), due to the greater thermal stability of bIm. The hybrid material shows an intermediate behaviour, with two decomposition steps corresponding to the coexistence of 4-m-5-ica and bIm in the framework structure, as previously demonstrated by NMR spectroscopy. However, the onset

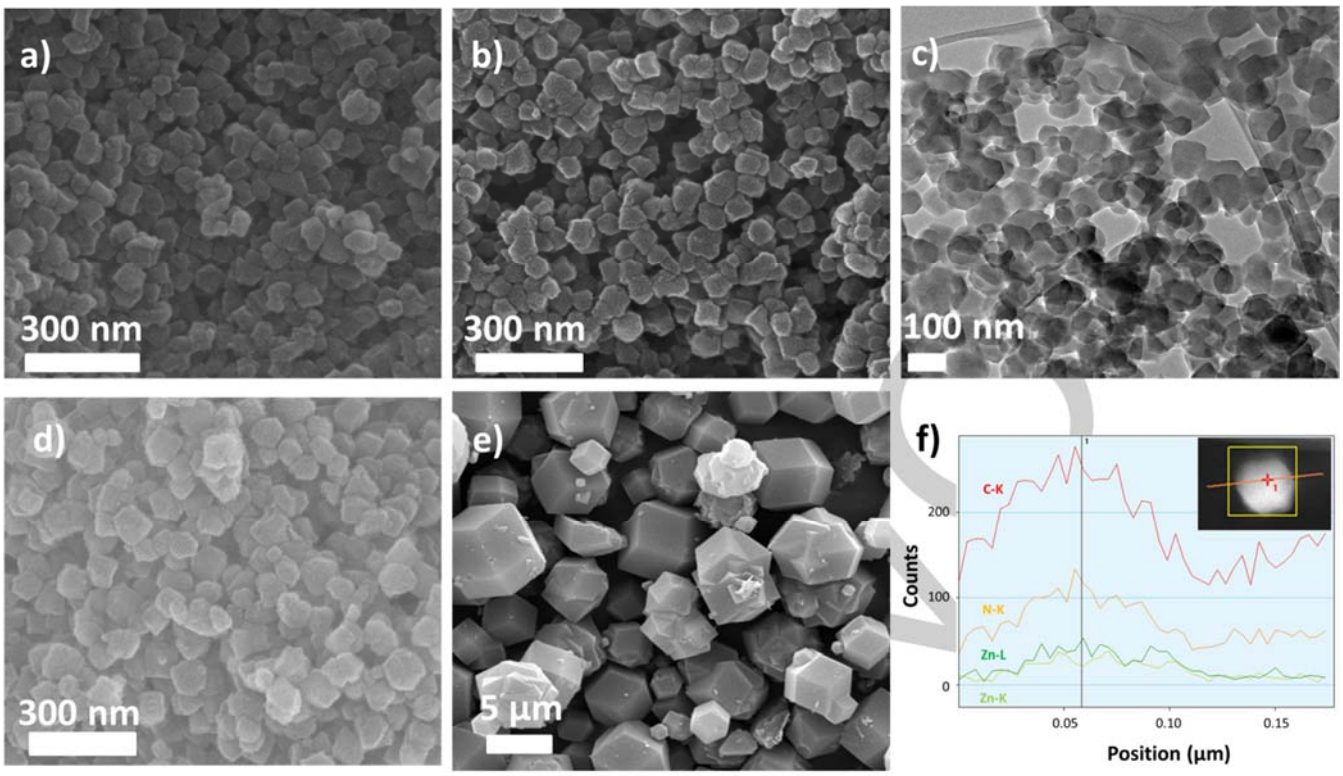

Figure 4. SEM images of ZIF-93 (a), ZIF-93/11 hybrid material (DMAc, b), ZIF-93/11 hybrid (MeOH, d) and ZIF-11 (e). Also TEM image of ZIF-93/11 hybrid material (DMAc, c) and TEM/EDX analysis of a single ZIF-93/11 hybrid nanoparticle synthesised in DMAc (f).

temperatures are slightly different to those of the neat ZIFs (384 vs. 366 ^{0}C for 4-m-5-ica and 498 vs. 576 ^{0}C for bIm). The 4-m-5-ica in the hybrid structure is, therefore, more stable than that in ZIF-93, whereas the bIm is more stable in ZIF-11 than in the hybrid material. Moreover, the degradation of the hybrid ZIF synthesised in MeOH is more similar to that of ZIF-93, in agreement with low amount of bIm in this hybrid. In any event, the existence of a continuous mass loss process that does not correspond to the superposition of the TGA curves of the two neat ZIFs is strongly indicative of the existence of a unique hybrid phase rather than a physical mixture of ZIF-93 and ZIF-11. Moreover, the weight loss regarding water adsorption (5 wt%) is much lower than that in ZIF-93, what means that a small amount of bIm (7.4% for the MeOH hybrid) is enough to increase somehow the hydrophobicity.

Figures 4a-d show the SEM/TEM images of ZIF-93 and ZIF-93/11 hybrid nanoparticles, whereby the similar morphology and particle sizes are observed. A narrow particle size distribution (around 72-73 nm for all the three ZIFs according to the cumulative distribution graph of Figure S3) can be observed suggesting the existence of just one phase (*i.e.* a hybrid material, instead of a physical mixture of ZIF-93 and ZIF-11). Figure 4e shows the SEM image of the micro-sized ZIF-11 resulting from the chosen synthetic route. EDX analysis was performed on a single nanoparticle of ZIF-93/11 synthesised in DMAc, revealing, upon discounting the composition variation due to particle geometry, that the Zn and N amounts remain constant across the particle width (Figure 4f).

The XRD patterns of the ZIF-93/11 hybrid material, ZIF-11 and ZIF-93 are shown in Figure S4 for comparison. Both ZIF-93 and ZIF-11 have a rhombohedral topology, showing similar diffractograms, making distinction for the hybrid material by XRD difficult. No characteristic features are observed for the hybrid framework (synthesised in DMAc), which exhibits the same crystalline structure as ZIF-93. However, the ZIF synthesised in MeOH shows changes in some of the signal intensities. The peak at 4.3^0 (2θ) reduced its intensity by 90%, whilst the peak at 7.4^0 (2θ) increased in intensity and was the most intense signal in the pattern.

The IR spectra of ZIF-93, ZIF-11 and the hybrid materials are shown in Figure S5. ZIF-11 shows very intense bands in the 600-1800 cm^{-1} range. The peak at 1222 cm^{-1} is caused by the in-plane C-H deformation of the disubstituted benzimidazole, while the peak at 902 cm^{-1} is due to the C–H out-of-plane bending of single hydrogen in substituted benzene rings. Finally, the signal at 738 cm^{-1} is related to the imidazole in-plane ring bending.[36] ZIF-93 shows an intense band between 3000-3690 cm^{-1}, corresponding to the adsorbed water. Moreover, peaks at 1655 and 1629 cm^{-1} are related to the aldehyde group stretches of the 4-m-5-ica linker.[27] The spectra of the hybrid materials exhibit a combination of all the signals observed for ZIF-93 and ZIF-11, although some differences to the neat ZIFs spectra can be identified. Firstly, the vibration modes in the 3000-3690 cm^{-1} region have disappeared, showing that the hybrid framework is not as hygroscopic as ZIF-93. Secondly, the peak at 1629 cm^{-1} is not as intense. When comparing the spectra of both hybrid materials, the band at 738 cm^{-1} is less intense in the sample synthesised in MeOH perhaps

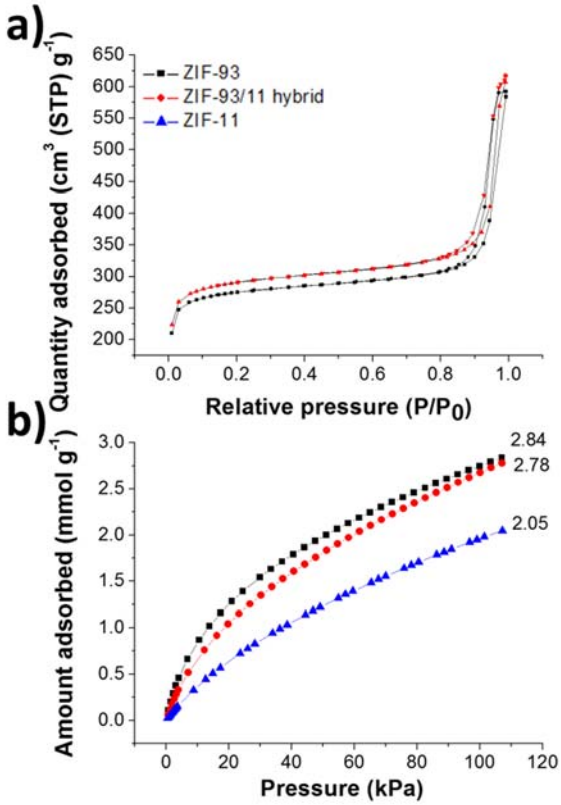

Figure 5. N_2 (77 K, a) and CO_2 adsorption (0 °C, b) isotherms of ZIF-93 (black), ZIF-11 (blue) and ZIF-93/11 hybrid material (synthesised in DMAc, red).

as a consequence of the lower amount of bIm in the material (see Table S1).

N_2 isotherms at 77 K were measured for ZIF-93 and the ZIF-93/11 hybrid material (synthesised in DMAc, it had the highest amount of bIm) to study their porosity (Figure 5a). ZIF-11 was deemed non-porous to N_2 (77 K) in this relative pressure range especially since it has narrow microporosity and a pore aperture size smaller than the kinetic diameter of N_2 (0.36 nm).[37] ZIF-93 shows a N_2 uptake of around 290 cm^3 (STP) g^{-1} at P/P_0=1 and a BET specific surface area of 980 m^2 g^{-1}. The ZIF-93/11 hybrid material performed slightly inferior values (274 cm^3 (STP) g^{-1} and 926 m^2 g^{-1}, respectively). According to their shape, both isotherms can be classified as Type I, typical of microporous materials. The inclusion of bIm in the ZIF-93 framework structure has very little effect on the amount of N_2 adsorbed relative to ZIF-93. This suggests that a perfect core of ZIF-11 was not obtained, in agreement with the lack of a sharp border separating both ZIF structures, above mentioned when dealing with the NMR characterization. Regarding the CO_2 adsorption at 0 ^{0}C (Figure 5b), ZIF-93 shows an uptake of 2.84 mmol g^{-1}, which is 39% higher than that of ZIF-11. For the ZIF-93/11 hybrid material, only a slight reduction in the amount of CO_2 adsorbed was observed (~2% relative to ZIF-93). These results are further confirmed for the CO_2 calorimetry measurements at 30 °C, reaching higher pressures to explore the adsorption capacities of the frameworks in greater detail (Figure 6a). In this case the ZIF-93/11 hybrid material showed intermediate CO_2 uptakes (1.37 mmol g^{-1} at 1 bar and 4.43 mmol g^{-1} at 10 bar) between those of the neat ZIFs. Interestingly, the calorimetry signal can be used to calculate the enthalpies of adsorption and the two pure ZIF samples show quite different behaviours (see Figure 6b). The initial enthalpy observed with ZIF-93 is at around 35 kJ mol^{-1} and decreases to around 25 kJ mol^{-1} and this can be interpreted by a slightly homogeneous surface with some different sorption centres. The ZIF-11 however, shows a flatter energy profile in the region of 25 kJ mol^{-1} suggesting a more homogeneous surface. The enthalpy signal observed with the hybrid material closely resembles that of the ZIF-93 suggesting that this phase is dominant with respect to the CO_2.

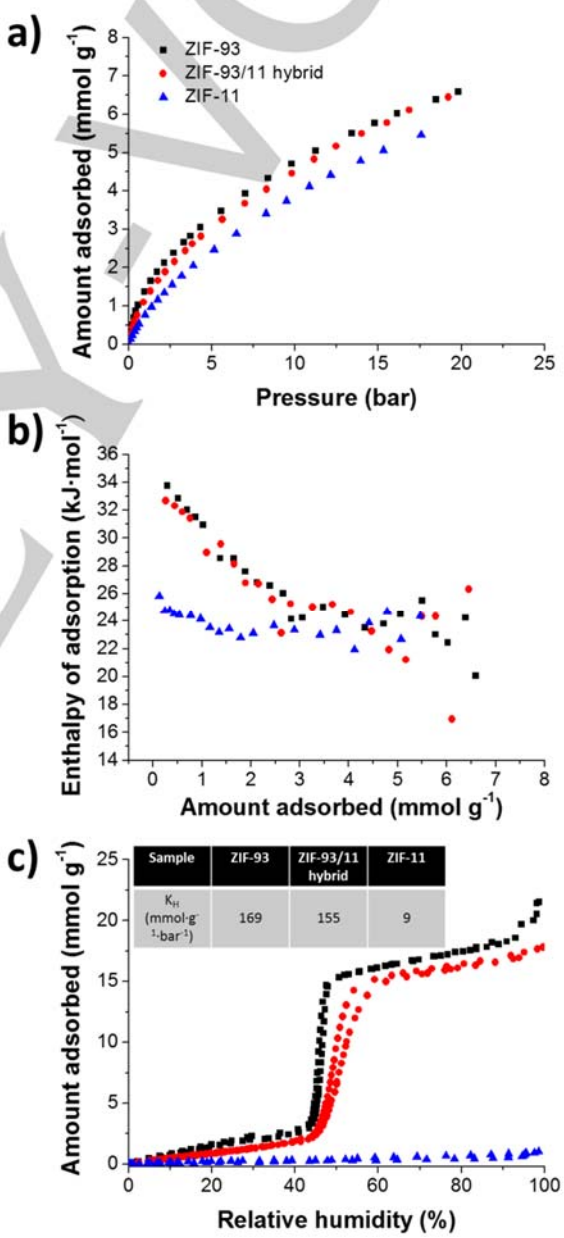

Figure 6. CO_2 adsorption at 30 ^{0}C (a) of ZIF-93 (black), ZIF-93/11 hybrid material (synthesised in DMAc) (red) and ZIF-11 (blue); CO_2 adsorption enthalpies (b); and H_2O adsorption at 25 ^{0}C (c).

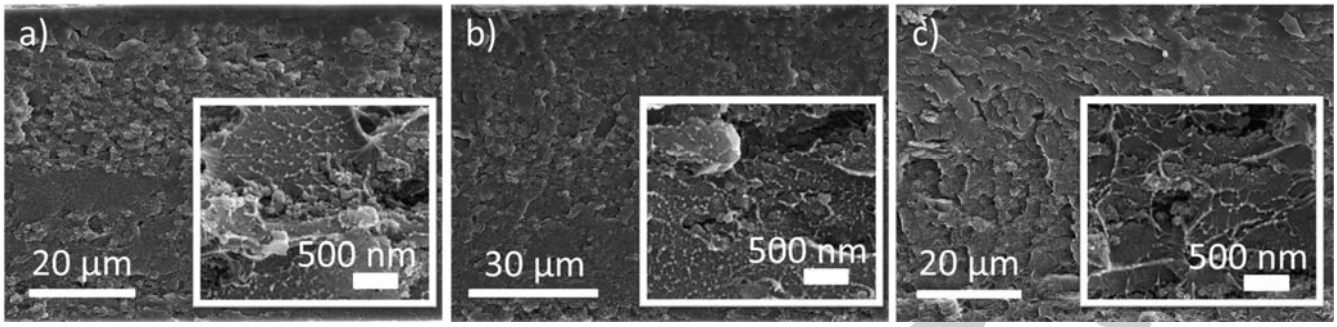

Figure 7. SEM images of the cross-sections of PBI membranes containing 20 wt% loading of ZIF-93 (a), ZIF-93/11 hybrid material (synthesised in DMAc) (b), and ZIF-93/11 hybrid material (synthesised in MeOH) (c).

Water adsorption analyses at 25 ^{0}C were performed on ZIF-93, ZIF-11 and the ZIF-93/11 hybrid material (Figure 6c). Whilst the pure ZIF-11 shows very little uptake throughout the experiment, the pure ZIF-93 is clearly a hygroscopic material, showing a water uptake over 20 mmol g^{-1} at a relative humidity of 95 %. The Henry constants, obtained at low coverage give an idea of the strength of interaction between the water and the various samples and again, this highlights that the ZIF-93 (k_H = 169 mmol g^{-1}·bar^{-1}) is a far more hydrophilic surface for water when compared to pure ZIF-11 (k_H = 9 mmol g^{-1}·bar^{-1}). There is a marked, and quite sharp, pore filling step observed with the ZIF-93 in the region of RH = 40-50 %. The hybrid material presents a water isotherm which resembles more the ZIF-93 material, however, with lower overall uptake and Henry constant (k_H = 155 mmol g^{-1}·bar^{-1}), even though the presence of hydrophobic bIm linker was as high as 23%. The pore filling step observed with the hybrid material seems to be slightly shifted to higher relative humidity and takes place over a slightly larger domain of relative humidity. These observations can be related to the influence of the incorporated bIm and are in agreement with TGA and FTIR analyses (Figures 3 and S5, respectively)

3.2 MMMs characterisation and gas separation performance

In order to test the gas separation capacity of the different hybrid frameworks, PBI MMMs with 20 wt% loading were prepared with the ZIF-93/11 hybrid materials synthesised in DMAc and MeOH. This 20 wt% loading was in agreement with previous analogous MMMs with ZIFs. [24],[33] ZIF-93 and ZIF-11 MMMs were also prepared for comparison. The morphology of the cross-section of these membranes is shown in Figure 7 (while the whole characterization of ZIF-11-PBI MMMs can be found in a previous work)[33], where a good dispersion and filler-polymer compatibility are observed.

All the membranes were tested at 180 ^{0}C and 3 bar of feed pressure for the separation of equimolar H_2/CO_2 mixture and the results in the Robeson type graph are shown in Figure 8. As the Robeson upper bound was originally defined at 35 ^{0}C, a correction for the elevated temperature was applied to acquire a more accurate bound. The upper bound shifts with the temperature according to equation 1:[38]

$$\alpha_{H_2/CO_2} = \frac{k \cdot e^{\gamma/T}}{P_{H_2}^n} \quad (equation\ 1)$$

where γ indicates the effect of temperature (in K) on the solubility and diffusivity of H_2 and CO_2, and k and n are the parameters that define the Robeson bound equation for this gas mixture (229 Barrer and 0.429, respectively). For H_2 and CO_2 in polymers, γ has a value of -543 K.[38] Increasing the temperature increases the upper bound, but has no effect on the selectivity-permeability slope.

For all of the MMMs the gas separation performances improved in comparison with that of the bare PBI membranes. Comparing the MMMs containing pure ZIFs, the ZIF-11 MMMs showed a H_2 permeability of 128 Barrer and a H_2/CO_2 selectivity of 4.9, while ZIF-93 MMMs were better (267 Barrer and 5.8, respectively). The MMMs containing the hybrid materials synthesised in MeOH had the highest gas separation performance reaching H_2 permeability values of 207 Barrer and 7.7 for H_2/CO_2 selectivity, which surpasses the Robeson upper bound, even when corrected for 180 ^{0}C. The larger amount of bIm in the hybrid material

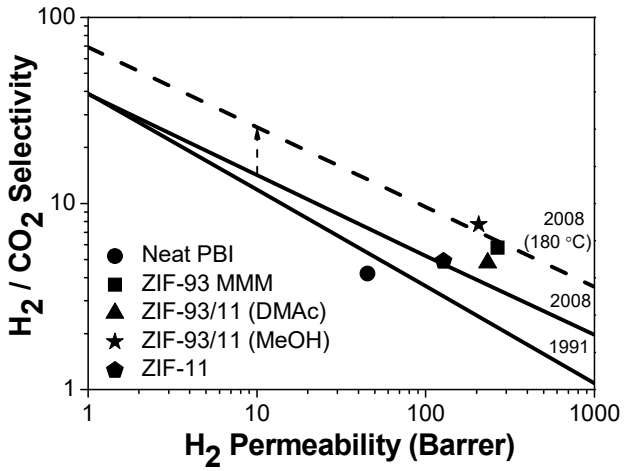

Figure 8. Gas separation performance of bare PBI membranes and 20 wt% loaded MMMs containing ZIF-93, ZIF-11 and the ZIF-93/11 hybrid materials synthesised in DMAc and MeOH. The continuous lines correspond to the original Robeson upper bounds of 1991[39] and 2008[40] and the dashed line corresponds to the upper bound calculated for 180 ^{0}C.

synthesised in DMAc may have led to the reduced performance of the corresponding MMM, since ZIF-93 was shown to have a better H_2/CO_2 separation than ZIF-11. In other words, only a small amount of bIm (7.4 % of total ligand achieved with MeOH treatment) is enough to improve the compatibility with the polymer (as in case of ZIF-11-PBI MMMs)[33] and constrain somehow the microporosity of the ZIF while maintaining a high value of open porosity. All this together makes the ZIF-93/11 hybrid material a suitable filler for the application of MMMs in the H_2/CO_2 mixture separation.

Finally, the industrial application of these membranes for H_2/CO_2 separation would involve some content of water in the feed stream. This water may cause competition for permeation paths through the membrane, decreasing the permeability of H_2. Future work would imply permeation tests with a high water activity in the feed to quantify whether the high water activity affects the membrane separation performance.

Conclusions

Two hybrid frameworks (with 7.4 and 23 % bIm) sharing features of ZIF-93 and ZIF-11 have been obtained *via* the post-synthetic modification of ZIF-93 nanoparticles in MeOH and DMAc. The use of these two solvents leads to a different proportion of bIm and 4-m-5-ica in the final hybrid material, which was quantified by solution-state ^{1}H NMR spectroscopy. The presence of both linkers was also verified by TGA analyses, proving also that the inclusion of bIm led to a stabilisation of the hybrid material. XPS analysis determined that both linkers were present on the surface of the nanoparticles, discarding the hypothesis of a core-shell type structure. The hybrid nanoparticles (72-73 nm) showed similar diffraction patterns to those of ZIF-93 and ZIF-11 and slight differences in their FTIR spectra according to the proportion of the two linkers in their structures. N_2 and CO_2 adsorption experiments showed a reduction in the adsorption capacity of the hybrid materials related to the presence of bIm in their structure. Similar results were acquired for the water adsorption capacities since the addition of bIm increases the hydrophobicity of the material. Both ZIF-93/11 hybrid materials were used as fillers in polymer PBI mixed matrix membranes that were tested for the separation of H_2/CO_2 mixtures at high temperatures. Loadings of 20 wt% for the hybrid materials showed better results (207 Barrer of H_2 and a H_2/CO_2 selectivity of 7.7 at 180 ^{0}C) than PBI membranes containing ZIF-93 and ZIF-11 at the same loadings.

Experimental Section

Chemicals. Benzimidazole (bIm, $C_7H_6N_2$, 98%), zinc acetate dihydrate ($Zn(CH_3COO)_2{\cdot}2H_2O$), N,N-dimethylacetamide (DMAc, ≥99.5 %), ammonium hydroxide (NH_4OH, 28-30% aqueous solution), chloroform (anhydrous), toluene (≥99.5%) and trimethylamine (≥99.5 %) were purchased from Sigma Aldrich. Methanol (MeOH, HPLC grade) was purchased from Scharlau. Commercial PBI solution comprising 26 wt% PBI with 1.5 wt% LiCl as stabilizer in DMAc was purchased from PBI Performance Products.

MOFs synthesis. Zn(CH3COO)2·2H2O (1.76 g, 8 mmol) was dissolved (room temperature, 15 min) in MeOH (80 mL). The linker 4-m-5-ica (1.76 g, 16 mmol) was dissolved (room temperature, 15 min) in water (200 mL). The linker/water solution was added to the Zn precursor/methanol solution followed by dropwise addition (room temperature) of trimethylamine (0.8 mL). The mixture gradually turned from clear to cloudy white. The mixture was stirred and heated (80 °C, 2 h), then allowed to cool to room temperature (15 min). The product was collected by centrifugation (15,000 rpm, 20 min) and washed with water for eight cycles. The white powder product was dried in air (room temperature, overnight). The resulting nanoparticles of ZIF-93 were ~73 nm wide.

The ZIF-93/11 hybrid material was prepared via post-synthetic modification of ZIF-93 in two different solvents: DMAc and MeOH. For the first synthesis, bIm (1.25 g, 11 mmol) was dissolved in DMAc (30 mL) and ZIF-93 (0.2 g, 0.7 mmol) was added to the solution. The suspension was stirred (30 °C, 3 days). The solid was collected by centrifugation, washed with MeOH under reflux (18 h), cooled, collected by centrifugation again and then dried (110 °C, overnight). For synthesis in MeOH, bIm (1.25 g, 11 mmol) was dissolved in a mixture of MeOH (6.4 g, 400 mmol), toluene (9.2 g, 100 mmol) and NH_4OH (2.4 g, 40 mmol). Then, ZIF-93 (0.2 g, 0.7 mmol) was added to the solution. The suspension was stirred (30 °C, 3 h) and the solid was collected by centrifugation and washed 3 times with MeOH. This solid was then dried (110 °C, overnight).

ZIF-11 was also prepared for comparison, following a literature method.[41] The linker, bIm (0.24 g, 2 mmol) was dissolved in a mixture of MeOH (6.4 g, 400 mmol), toluene (9.2 g, 100 mmol) and NH_4OH (2.4 g, 40 mmol). $Zn(CH_3COO)_2{\cdot}2H_2O$ (0.22 g, 1 mmol) was dissolved in methanol (3.2 g, 200 mmol). Both solutions were mixed and stirred (room temperature, 3 h). The resulting solid was collected by centrifugation, washed with MeOH three times for the complete removal of toluene and dried (100 °C, overnight). This synthesis results in micro-sized particles, which are larger than those of ZIF-93.

MMM preparation. The required amount of ZIF (ZIF-93/11 hybrid, ZIF-11 and ZIF-93) was weighed for a 20 wt% membrane loading. The corresponding amount of PBI solution (15 wt% in DMAc to reduce the viscosity) was added and the resulting solution was stirred overnight. The casting solution was subjected to three cycles of alternating stirring and sonication (90 min total treatment time) and then cast into Petri dishes (kept level) inside an oven (90 °C). The Petri dishes were left uncovered overnight to allow the evaporation of the solvent. Subsequently, the membranes were peeled off from the Petri dishes and washed with water (80 ºC, 4 h) and then dried in an oven (100 °C, 24 h).

The membrane thicknesses were measured with a Digimatic micrometer (measurement range 0-30 mm with an accuracy of ±1 µm). Nine equally distributed sites on each membrane were measured and the arithmetic mean was taken as the membrane thickness. The MMMs obtained in this work had a thickness of 78±2 µm. For permeation testing of the membranes, circular areas of 3.14 cm^2 were cut from the films.

Characterisation of samples. Powder X-ray diffraction (XRD) patterns of the MOFs were acquired using a D-Max Rigaku X-ray diffractometer with a copper anode and a graphite monochromator to select CuK_α radiation (λ = 1.540 Å), taking data from 2.5 to 40° (2θ) at a scan rate of 0.03 ^{0}s^{-1}. Thermogravimetric analyses (TGA) were carried out using a Mettler Toledo TGA/STDA 851e. Samples (5 mg) were placed in 70 µL alumina pans, which were heated in an air flow from 30 to 900 ^{0}C at a heating rate of 10 ^{0}C min^{-1}. Scanning electron microscopy (SEM) images of the ZIFs and membranes were obtained using an Inspect F50 model scanning electron microscope (FEI), operated at 20 kV. Cross-sections of membranes were prepared by freeze-fracturing after immersion in liquid nitrogen and subsequent coating with Pt. Transmission electron microscopy (TEM, FEI TECNAI F30) images of the ZIF samples were acquired at an acceleration voltage of 300 kW. The TEM, fitted with a SuperTwin® lens allowing a point resolution of 1.9 Å, was also used for

EDS (X-ray Microanalysis). Samples were prepared by placing one drop of a dilute suspension of powder in MeOH on a holey carbon-coated copper grid (300 mesh) and allowing the solvent to evaporate (room temperature). Particle size was obtained using ImageJ 1.49b software, where at least 60 particles were counted for each sample. Fourier transform infrared (FTIR) spectroscopy was performed on a Bruker Vertex 70 FTIR spectrometer equipped with a DTGS detector and a Golden Gate diamond ATR accessory. Both spectra were recorded by averaging 40 scans in the 4000-600 cm^{-1} wavenumber range at a resolution of 4 cm^{-1}. Nitrogen adsorption/desorption isotherms were obtained using a Micromeritics Tristar 3000 surface area and porosity analyser, after previously degassing the samples (200 ^{0}C, vacuum, 8 h). CO_2 adsorption isotherms were measured using a volumetric adsorption analyser (Micromeritics ASAP 2020) at 0 ^{0}C up to 120 kPa after degassing (200 ^{0}C, 8 h). The N_2, CO_2 and He gases used in the experiments were 99.9995% pure.

Solution-state ^{1}H nuclear magnetic resonance (^{1}H NMR) spectra were acquired using a Bruker Avance 500 (500 MHz) spectrometer at ambient temperature. The samples were digested in deuterated DMSO with the addition of concentrated HCl (37%) to aid dissolution. Chemical shifts (δ) are reported in parts per million (ppm) relative to tetramethylsilane (TMS). Solid-state ^{13}C magic angle spinning (MAS) NMR spectra were recorded on a Bruker Avance III spectrometer equipped with a 9.4 T wide-bore superconducting magnet (Larmor frequencies of 400.13 and 100.61 MHz for ^{1}H and ^{13}C, respectively). Samples were packed into zirconia rotors with an outer diameter of 4 mm and rotated at the magic angle at a rate of 12.5 kHz. Spectra were recorded with cross polarisation (CP) from ^{1}H with a contact pulse (ramped for ^{1}H) of 1 ms. High-power (v1 ~100 kHz) two-pulse phase modulation (TPPM) decoupling of ^{1}H was applied during acquisition. Signal averaging was carried out for 2048-4096 transients with a recycle interval of 3 s. Chemical shifts are reported in ppm relative to TMS using the CH_3 resonance of L-alanine (δ = 20.5 ppm) as a secondary reference.

The XPS spectra were collected on a Scienta 300 XPS spectrometer working at a base pressure <5x10^{-9} mbar. Monochromated Al K_α X-rays were used throughout, generated from a rotating anode source operating at approximately 4 kW power. Wide energy survey scans were performed to determine the elements present (2 scans, dwell time 200 ms and 200 meV step size) before more detailed scans were performed on the regions of interest (2 scans, dwell time 533 ms and 20 meV step size). A pass energy of 150 eV was used throughout and the energy scale referenced to Au4f_7 at 83.95 eV binding energy. The signals were collected by a multichannel plate/phosphor screen/video camera combination and all spectra were analysed using the Casa XPS software.

Adsorption enthalpies were measured experimentally using a Tian-Calvet type microcalorimeter coupled with a home-made manometric gas dosing system.[42] This apparatus allows the simultaneous measurement of the adsorption isotherm and the corresponding differential enthalpies. Gas is introduced into the system using a step-by-step method and each dose is allowed to stabilize in a reference volume before being brought into contact with the adsorbent located in the microcalorimeter. The introduction of the adsorbate to the sample is accompanied by an exothermic thermal signal, measured by the thermopiles of the microcalorimeter. The peak in the calorimetric signal is integrated over time to give the total energy released during this adsorption step. At low coverage the error in the signal can be estimated to around ±0.2 kJ mol^{-1}.

Around 0.3 g of sample was used and was outgassed at 150 °C for 16 h under secondary vacuum prior to each experiment. For each injection of gas, equilibrium was assumed to have been reached after 90 min. This was confirmed by the return of the calorimetric signal to its baseline (<5 µW). The gas used for the adsorption was obtained from Air Liquide (99.997% purity).

Gas separation analysis. Mixed gas analyses were performed for PBI MMMs containing a 20 wt% loading of both ZIF-93/11 hybrid materials. The membranes were placed in a module comprised of two stainless steel pieces and a 316L SS macroporous disk support (from Mott Co.) with a 20 µm nominal pore size, and gripped inside with Viton O-rings. The permeation module was placed in a UNE 200 Memmert oven to control the temperature of the experiments (180 ºC). Gas separation measurements were carried out by feeding an equimolar mixture of H_2/CO_2 (25/25 cm^3(STP)min^{-1}) at 3 bar to the feed side by means of two mass-flow controllers (Alicat Scientific, MC-100CCM-D), while the permeate side of the membrane was swept with a 2 cm^3(STP)min^{-1} mass-flow controller stream of Ar at 1 bar (Alicat Scientific, MC-5CCM-D). Concentrations of H_2 and CO_2 in the outgoing streams were analysed by an Agilent 3000A online gas microchromatograph equipped with a thermal conductivity detector. Permeability was calculated in Barrer (1×10^{-10} cm^3(STP)·cm/(cm^2·s·cmHg)) once the steady-state of the exit stream was reached (for at least 3 h), and the separation selectivity was calculated as the ratio of permeabilities. The membranes had to be handle with case because of the brittleness of PBI. This was truer for the MMMs, and they had to be cut carefully. In any event, the literature shows how brittle membranes have greater processability in the form of supported membranes, where thin selective layers are deposited on high performance polymeric supports that provide mechanical stability, solving the problem.[43]

Acknowledgements

The research leading to these results has received funding from the European Union Seventh Framework Programme (FP7/2007-2013) under grant agreement n° 608490, project M4CO2. In addition, financial support from the Spanish MINECO and FEDER (MAT2016-77290-R), the Aragón Government (T05) and the ESF is gratefully acknowledged. J. S.-L. thanks the Spanish Education Ministry Program FPU2014 for his PhD grant. All the microscopy work was done in the Laboratorio de Microscopías Avanzadas at the Instituto de Nanociencia de Aragón (LMA-INA). The authors would like to acknowledge the use of the Servicio General de Apoyo a la Investigación-SAI, Universidad de Zaragoza. Prof. Dr. Steven Abbott is thanked for providing Hansen solubility parameters.

Keywords: hybrid zeolitic imidazolate framework • synthesis design • membranes • polybenzimidazole• H_2/CO_2 separation

[1] G. Ferey, C. Serre, *Chem. Soc. Rev.* **2009**, *38*, 1380-1399.

[2] a) B. Zornoza, C. Tellez, J. Coronas, J. Gascon, F. Kapteijn, *Microporous Mesoporous Mater.* **2013**, *166*, 67-78. b) H. B. T. Jeazet, C. Staudt, C. Janiak, *Dalton Transactions* **2012**, *41*, 14003-14027.

[3] P. Horcajada, C. Serre, M. Vallet-Regí, M. Sebban, F. Taulelle, G. Férey, *Angew. Chem.* **2006**, *118*, 6120-6124, *Angew. Chem. Int. Ed.* **2006**, *45*, 5974-5978.

[4] a) H. Jiang, T. Akita, T. Ishida, M. Haruta, Q. Xu, *J. Am. Chem. Soc.* **2011**, *133*, 1304-1306. B) J. Gascon, U. Aktay, M. D. Hernandez-Alonso, G. P. M. van Klink, F. Kapteijn, *J. Catal.* **2009**, *261*, 75-87.

[5] K. S. Park, Z. N. Ni, A. P. Cô te, J. Y. Choi, R. Huang, F. J. Uribe-Romo, H. K. Chae, M. O'Keeffe, O. M. Yaghi, *PNAS* **2006**, *103*, 10186-10191.

[6] J. A. Thompson, C. R. Blad, N. A. Brunelli, M. E. Lydon, R. P. Lively, C. W. Jones, S. Nair, *Chem.Mater.* **2012**, *24*, 1930-1936.

[7] C. Zhang, Y. Xiao, D. Liu, Q. Yang, C. Zhong, *Chem. Commun.* **2013**, *49*, 600-602.

[8] R. Banerjee, A. Phan, B. Wang, C. Knobler, H. Furukawa, M. O'Keeffe, O. M. Yaghi, *Science* **2008**, *319*, 939-943.

[9] R. Banerjee, H. Furukawa, D. Britt, C. Knobler, M. O'Keeffe, O. M. Yaghi, *J. Am. Chem. Soc.* **2009**, *131*, 3875-3877.

[10] N. T. Nguyen, H. Furukawa, F. Gándara, H. T. Nguyen, K. E. Cordova, O. M. Yaghi, *Angew. Chem. Int. Ed.* **2014**, *53*, 10645-10648.
[11] S. M. Cohen, *Chem. Rev.* **2011**, *112*, 970-1000.
[12] a) Z. Wang, S. M. Cohen, *J. Am. Chem. Soc.* **2007**, *129*, 12368-12369. b) K. K. Tanabe, Z. Wang, S. M. Cohen, *J. Am. Chem. Soc.* **2008**, *130*, 8508-8517. c) M. J. Ingleson, J. P. Barrio, J. Guilbaud, Y. Z. Khimyak, M. J. Rosseinsky, *Chem. Commun.* **2008**, 2680-2682. d) S. J. Garibay, Z. Wang, K. K. Tanabe, S. M. Cohen, *Inorg. Chem.* **2009**, *48*, 7341-7349. e) Z. Wang, S. M. Cohen, *Angewandte Chemie* **2008**, *120*, 4777-4780. f) D. Britt, C. Lee, F. J. Uribe-Romo, H. Furukawa, O. M. Yaghi, *Inorg. Chem.* **2010**, *49*, 6387-6389.
[13]13 M. Meilikhov, K. Yusenko, R. A. Fischer, *J. Am. Chem. Soc.* **2009**, *131*, 9644-9645.
[14] a) T. Ahnfeldt, D. Gunzelmann, T. Loiseau, D. Hirsemann, J. Senker, G. Férey, N. Stock, *Inorg. Chem.* **2009**, *48*, 3057-3064. b) C. Volkringer, S. M. Cohen, *Angew. Chem. Int. Ed.* **2010**, *49*, 4644-4648. c) S. J. Garibay, Z. Wang, S. M. Cohen, *Inorg. Chem.* **2010**, *49*, 8086-8091.
[15] K. M. Taylor-Pashow, J. D. Rocca, Z. Xie, S. Tran, W. Lin, *J. Am. Chem. Soc.* **2009**, *131*, 14261-14263.
[16] S. Bernt, V. Guillerm, C. Serre, N. Stock, *Chemical Communications* **2011**, *47*, 2838-2840.
[17] a) V. Guillerm, F. Ragon, M. Dan-Hardi, T. Devic, M. Vishnuvarthan, B. Campo, A. Vimont, G. Clet, Q. Yang, G. Maurin, *Angew. Chem. Int. Ed.* **2012**, *51*, 9267-9271. b) M. Kandiah, S. Usseglio, S. Svelle, U. Olsbye, K. P. Lillerud, M. Tilset, *J. Mater. Chem.* **2010**, *20*, 9848-9851.
[18] S. J. Garibay, S. M. Cohen, *Chem. Commun.* **2010**, *46*, 7700-7702.
[19] S. S. Chui, S. M. Lo, J. P. Charmant, A. G. Orpen, I. D. Williams, *Science* **1999**, *283*, 1148-1150.
[20] A. Huang, J. Caro, *Angew. Chem. Int. Ed.* **2011**, *50*, 4979-4982.
[21] J. Canivet, S. Aguado, C. Daniel, D. Farrusseng, *ChemCatChem* **2011**, *3*, 675-678.
[22] F. Cacho-Bailo, M. Etxeberría-Benavides, O. Karvan, C. Téllez, J. Coronas, *CrystEngComm* **2017**, *19*, 1545-1554.
[23] X. Liu, Y. Li, Y. Ban, Y. Peng, H. Jin, H. Bux, L. Xu, J. Caro, W. Yang, *Chem. Commun.* **2013**, *49*, 9140-9142.
[24] J. Sánchez-Laínez, A. Veiga, B. Zornoza, S. R. Balestra, S. Hamad, A. R. Ruiz-Salvador, S. Calero, C. Téllez, J. Coronas, *J. Mater. Chem. A* **2017**, 5, 25601–25608.
[25] A. W. Thornton, D. Dubbeldam, M. S. Liu, B. P. Ladewig, A. J. Hilla, M. R. Hill, *Energy Environ. Sci.* **2012**, *5*, 7637–7646.
[26] K. G. Ray, D. L. Olmsted, J. M. Burton, Y. Houndonougbo, B. B. Laird, M. Asta, *Chem. Mater.* **2014**, *26*, 3976-3985.
[27] W. Morris, B. Leung, H. Furukawa, O. K. Yaghi, N. He, H. Hayashi, Y. Houndonougbo, M. Asta, B. B. Laird, O. M. Yaghi, *J. Am. Chem. Soc.* **2010**, *132*, 11006-11008.
[38]28 P. Bernardo, E. Drioli, G. Golemme, *Ind Eng Chem Res* **2009**, *48*, 4638-4663.
[29] a) T. Chung, L. Y. Jiang, Y. Li, S. Kulprathipanja, *Prog. Polymer Sci.***2007**, *32*, 483-507. b) P. Goh, A. Ismail, S. Sanip, B. Ng, M. Aziz, *Separation Purification Technol.* **2011**, *81*, 243-264.
[30] a) S. Choi, J. Coronas, Z. Lai, D. Yust, F. Onorato, M. Tsapatsis, *J. Membr. Sci.* **2008**, *316*, 145-152. b) T. Yang, Y. Xiao, T. Chung, *Energy Environ. Sci.* **2011**, *4*, 4171-4180. c) L. Li, Y. Jianfeng, X. Wang, Y. Chen, H. Wang, *J. Appl. Polym. Sci.* **2014**, *131*, 41056. d) X. Li, R. P. Singh, K. W. Dudeck, K. A. Berchtold, B. C. Benicewicz, *J. Membr. Sci.* **2014**, *461*, 59-68. e) S. Kumbharkar, Y. Liu, K. Li, *J. Membr. Sci.* **2011**, *375*, 231-240. f) B. P. Biswal, A. Bhaskar, R. Banerjee, U. K. Kharul, *Nanoscale* **2015**, *7*, 7291-7298.
[31] T. Chung, *J. Macromol. Sci., Part C: Polymer Reviews* **1997**, *37*, 277-301.
[32] a) T. Yang, G. M. Shi, T. Chung, *Adv. Energy Mater.* **2012**, *2*, 1358-1367. b) T. Yang, T. Chung, *Int. J. Hydrogen Energy* **2013**, *38*, 229-239. c) A. Bhaskar, R. Banerjee, U. Kharul, *J. Mater. Chem. A* **2014**, *2*, 12962-12967.
[33] J. Sánchez-Laínez, B. Zornoza, C. Téllez, J. Coronas, *J. Mater. Chem. A* **2016**, *4*, 14334-14341.
[34] T. Yang, T. Chung, *J. Mater. Chem. A* **2013**, *1*, 6081-6090.
[35] C. M. Hansen, *Prog. Org. Coat.* **2004**, *51*, 77-84.
[36] D. P. Drolet, D. M. Manuta, A. J. Lees, A. Katnani, G. J. Coyle, *Inorg. Chim. Acta* **1988**, *146*, 173-180.
[37] W. Morris, N. He, K. G. Ray, P. Klonowski, F. Hiroyasu, I. N. Daniels, Y. A. Houndonougbo, M. Asta, O. M. Yaghi, B. B. Laird, *J. Phys. Chem.* **2012**, *116*, 24084−24090.
[38] B. W. Rowe, L. M. Robeson, B. D. Freeman, D. R. Paul, *J. Membr. Sci.* **2010**, *360*, 58-69.
[39] L. M. Robeson, *J. Membr. Sci.*, **1991,** *62*, 165-185
[40] L. M. Robeson, *J. Membr. Sci.,* **2008**, *320*, 390-400.
[41] M. He, J. Yao, Q. Liu, Z. Zhongb, H. Wang, *Dalton Trans.* **2013**, *42*, 16608-16608–16613.
[42] P. L. Llewellyn, G. Maurin, *Comptes Rendus Chimie* **2005**, *8*, 283-302.
[43] Z. Dai, L. Ansaloni, L. Deng, *Green Energy Environ.,* **2016,** *1,* 102-128.

Entry for the Table of Contents

FULL PAPER

The synthesis of ZIF-93/11 hybrid nanoparticles by post-synthetic modification of ZIF-93 is shown in this work. These frameworks, with the **rho** topology, are based on a mixture of bIm and 4-m-5-ica in different proportions. They have been applied as fillers in polybenzimidazole mixed matrix membranes, which have been tested for the H_2/CO_2 separation at 180 ^{0}C, reaching optimal values of 207 Barrer of H_2 and a H_2/CO_2 selectivity of 7.7 that clearly surpassed the Robeson upper bound.

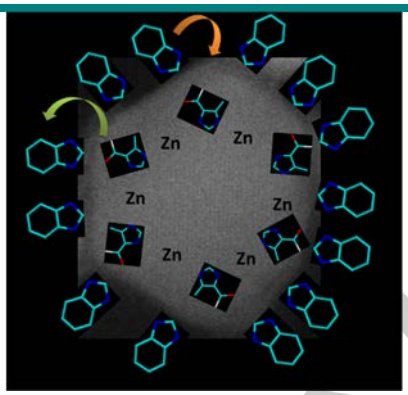

J. Sánchez-Laínez,[a] Dr. B. Zornoza,[a] Dr. A. F. Orsi,[b] M. M. Łozińska, [b] D. M. Dawson, [b] Prof. S. E. Ashbrook, [b] S. M. Francis, [b] Prof. Dr. P. A. Wright, [b] Dr. V. Benoit,[c] Dr. P. L. Llewellyn,[c] Prof. Dr. C. Téllez[a] and Prof. Dr. J. Coronas[a]*

Page No. – Page No.

Synthesis of ZIF-93/11 Hybrid Nanoparticles via Post-synthetic modification of ZIF-93 and their Use for H_2/CO_2 Separation